

# High-order harmonic spectroscopy for molecular imaging of polyatomic molecules

M. Negro,<sup>a</sup> M. Devetta,<sup>a</sup> D. Faccialá,<sup>b</sup> S. De Silvestri,<sup>b</sup> C. Vozzi<sup>\*a</sup> and S. Stagira<sup>b</sup>

Received 7th March 2014, Accepted 12th May 2014

DOI: 10.1039/c4fd00033a

High-order harmonic generation is a powerful and sensitive tool for probing atomic and molecular structures, combining in the same measurement an unprecedented attosecond temporal resolution with a high spatial resolution of the order of an angstrom. Imaging of the outermost molecular orbital by high-order harmonic generation has been limited for a long time to very simple molecules, like nitrogen. Recently we demonstrated a technique that overcame several of the issues that have prevented the extension of molecular orbital tomography to more complex species, showing that molecular imaging can be applied to a triatomic molecule like carbon dioxide. Here we report on the application of such a technique to nitrous oxide ( $\text{N}_2\text{O}$ ) and acetylene ( $\text{C}_2\text{H}_2$ ). This result represents a first step towards the imaging of fragile compounds, a category which includes most of the fundamental biological molecules.

## 1 Introduction

High order harmonic generation (HHG) occurs when atoms or molecules exposed to an intense femtosecond laser pulse are ionized by tunneling. The freed electron is then accelerated in the external electric field. Because of the periodic oscillation of the laser field the electron is brought back to the parent ion where it may recombine emitting an XUV photon.<sup>1</sup> This XUV radiation has been shown to contain information on the electronic structure of the emitting molecule and on its internal dynamics. Attosecond nuclear<sup>2</sup> and electronic dynamics<sup>3,4</sup> have been extracted from HHG in simple molecules and spectral features in the harmonic emission have been related to the molecular electronic structure and have been used for imaging the highest occupied molecular orbital (HOMO).

The idea of exploiting HHG for the tomographic reconstruction of molecular orbitals was first introduced by Itatani *et al.* in 2004 for the nitrogen molecule.<sup>5</sup> Since then, numerous experiments have been realized addressing the role of the

<sup>a</sup>Istituto di Fotonica e Nanotecnologie, CNR, 20133 Milan, Italy. E-mail: caterina.vozzi@ifn.cnr.it

<sup>b</sup>Dipartimento di Fisica, Politecnico di Milano, 20133 Milan, Italy

HOMO in the harmonic spectral intensity,<sup>6,7</sup> in the molecular-frame photo-ionization<sup>8</sup> and in the subsequent attosecond XUV emission,<sup>9</sup> as well as in the polarization state of the emitted radiation.<sup>10</sup> The dependence of the HHG process on the HOMO structure has also been exploited for the characterization in the time domain of the rotational<sup>11</sup> and vibrational<sup>12</sup> molecular excitations.

All these studies rely on two major assumptions: (i) the molecular HHG is dominated by the HOMO structure; (ii) the relationship between molecular structure and emitted XUV spectrum is simple and completely captured by the Strong Field Approximation (SFA), *i.e.* the electron quiver motion is not perturbed by the Coulomb potential of the ion. Both these assumptions have been recently put into question. Recent experiments have enlightened the role of multiple orbital contributions to HHG emission.<sup>3,4</sup> Furthermore, the influence of the Coulomb field of the parent ion in the generation of high order harmonics from molecules has been considered as a serious hindrance to a clear HOMO reconstruction.<sup>13</sup> To perform molecular tomography of more complex species one has to go beyond these assumptions.

As well as these two more fundamental obstacles, there are also additional, more technical difficulties. In order to retrieve the HOMO structure, one has to record the XUV harmonic spectra for different molecular orientations with respect to the laser field. Hence, it is necessary to fix the molecular orientation in space and change the polarization direction of the HHG-driving field.<sup>5</sup> Laser-assisted molecular alignment is a widespread technique able to accomplish this task,<sup>14</sup> but the molecular alignment achieved in this way is not ideal. Hence the experimental results and the corresponding HOMO tomography are affected by angular averaging effects. Moreover, in the case of non-linear molecules, the tomographic procedure requires to fix two or three angular coordinates of the molecule under investigation. For instance, the study of linear polar molecules requires the head-tail direction in space to be fixed. The feasibility of the laser assisted molecular orientation has been recently demonstrated<sup>15</sup> and exploited in HHG spectroscopy,<sup>16-18</sup> but no direct application to molecular imaging has been yet realized.

The amount of information that can be extracted from the harmonic emission depends on the spectral extension of the XUV radiation, that is known to scale with the so-called cut-off law:  $E_{\max} = I_p + 3.17U_p$ , where  $I_p$  is the ionization potential of the molecule and  $U_p$  is the ponderomotive energy of the electron in the laser field. This poses another important problem when HHG molecular imaging is extended to species with a low ionization potential (*i.e.* all organic molecules, and in particular those having important biological functions) as the extension emission spectrum is reduced. Since  $U_p \propto \lambda^2 I$ , where  $I$  is the peak intensity and  $\lambda$  the wavelength of the driving laser pulse, the emission cut-off may be extended by both increasing the field intensity or the laser wavelength. In this respect, standard Ti:sapphire laser sources generally used in HHG are not ideal candidates for tomography in fragile molecules, since the intense optical fields needed completely ionize the molecule before a well-developed XUV spectrum is generated.

To overcome the limitations posed by ionization saturation, the exploitation of mid-infrared driving sources has been demonstrated to be a powerful tool to extend harmonic emission far in the XUV.<sup>19-23</sup> With a mid-IR source<sup>24</sup> we recently demonstrated that it is possible to extend the spectral investigation in carbon

dioxide beyond 100 eV in the absence of multielectron effects, thus avoiding any ambiguity in the reconstructed wavefunction. In addition, by exploiting an all-optical non-interferometric technique, it was possible to trace both the spectral intensity and phase of the high order harmonics generated by single molecules as a function of the emitted photon energy and molecular angular orientation, without averaging effects. Furthermore, the tomographic procedure was generalized in order to take into account the Coulomb potential seen by the re-colliding electron wavepacket.<sup>25</sup>

In this work, we extend that approach to more complex molecules, such as N<sub>2</sub>O and C<sub>2</sub>H<sub>2</sub> pointing out some strengths and weaknesses of this investigation technique.

## 2 Experimental setup

We exploited an optical parametric amplifier (OPA) pumped by an amplified Ti:sapphire laser system (60 fs, 20 mJ, 800 nm). The OPA is based on difference frequency generation and provides driving pulses with a 1450 nm central wavelength, a pulse duration of 20 fs and a pulse energy of 1.2 mJ.<sup>24</sup> High harmonics were generated by focusing the mid-IR pulse in a supersonic gas jet under vacuum, due to the strong absorption exhibited by air in the XUV spectral region. The molecules in the jet were impulsively aligned with a portion of the fundamental 800 nm beam which was spectrally broadened by optical filamentation in an argon-filled gas cell and temporally stretched up to 100 fs by propagation through a glass plate. Such duration is required for achieving a good alignment of the molecular sample. In our experimental setup, the driving and aligning pulses were collinear and their polarizations were parallel. The delay between the two pulses was adjusted by means of a fine-resolution translation stage. The XUV radiation was acquired by means of a flat-field spectrometer and a multi-channel plate detector coupled to a CCD camera.<sup>26</sup>

## 3 Results

Harmonic spectra were acquired in N<sub>2</sub>O and C<sub>2</sub>H<sub>2</sub> as a function of the delay  $\tau$  between the aligning and driving pulse around the first rotational half revival ( $\tau_{N_2O} = 19.95$  ps and  $\tau_{C_2H_2} = 7.08$  ps). The results are shown in Fig. 1(a) and 2(a) for N<sub>2</sub>O and C<sub>2</sub>H<sub>2</sub> respectively. Fig. 1(b) and 2(b) show the corresponding calculated alignment factor for the experimental conditions.

In both molecules, the sequence of harmonic spectra shows a strong modulation with the delay  $\tau$  that can be ascribed to the dependence of the harmonic yield on the molecular orbital structure. In particular, a reduction of the harmonic emission can be observed for the delay corresponding to the maximum of the alignment factor and an enhancement of the harmonic yield appears for the minimum of the alignment factor. A major difference between the two cases is the presence of a region of harmonic enhancement at high photon energy, that appears in N<sub>2</sub>O at maximum alignment.

These effects can be naively interpreted in terms of a two-center interference occurring in the re-collision step.<sup>7,27</sup> If one considers a diatomic homo-nuclear molecule with a symmetric electronic state with respect to the nuclei exchange and assumes the re-colliding electron as a plane wave, the condition for

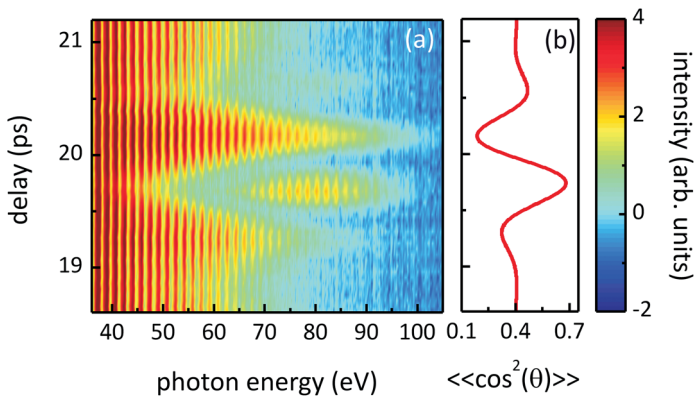


**Fig. 1** (a) Sequence of harmonic spectra measured in  $\text{N}_2\text{O}$  as a function of emitted photon energy and delay between the aligning and the driving pulse (log scale). (b) Calculated alignment factor for  $\text{N}_2\text{O}$  in the experimental conditions (rotational temperature 75 K, aligning pulse duration 100 fs, aligning pulse intensity  $3.32 \times 10^{13} \text{ W cm}^{-2}$ ).

constructive interference reads  $R\cos(\theta) = n\lambda_B$ , where  $R$  is the internuclear separation,  $\theta$  is the angle between the molecular axis and the electron wave-vector,  $n$  is an integer number and  $\lambda_B$  is the de Broglie wavelength associated to the re-colliding electron wave-packet. Similarly the condition for destructive interference is  $R\cos(\theta) = (n + 1/2)\lambda_B$  and the first destructive interference occurs for  $n = 0$ . The conditions become reversed for molecules with an antisymmetric electronic structure.

This concept can be extended to the molecules subject of our investigation. The acetylene molecule has a symmetric  $\pi$  HOMO in which the separation between the carbon atoms is  $R_{\text{C}\equiv\text{C}} = 1.2 \text{ \AA}$ . This is the distance that should be considered for the evaluation of the interference condition. The  $\text{N}_2\text{O}$  HOMO does

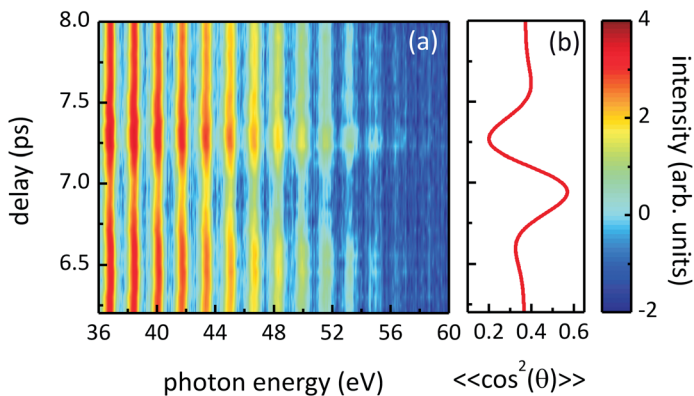


**Fig. 2** (a) Sequence of harmonic spectra measured in  $\text{C}_2\text{H}_2$  as a function of emitted photon energy and delay between the aligning and the driving pulse (log scale). (b) Calculated alignment factor for  $\text{C}_2\text{H}_2$  in the experimental conditions (rotational temperature 75 K, aligning pulse duration 100 fs, aligning pulse intensity  $2.16 \times 10^{13} \text{ W cm}^{-2}$ ).

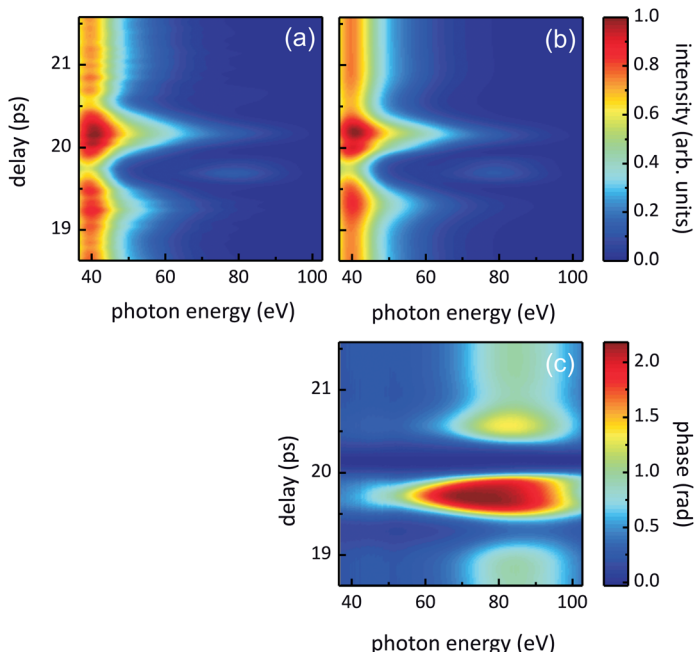
not have a clear symmetry, however in our experimental condition the harmonic spectra are acquired in aligned molecules and correspond to the average between the two possible orientation. The resulting signal can be interpreted in terms of emission from an effective molecular orbital similar to the anti-symmetric  $\pi$  orbital of CO<sub>2</sub>. In this view the overall length of this “effective” orbital is  $R_{N_2O} = 2.3 \text{ \AA}$ . Since  $R_{N_2O} \approx 2R_{C\equiv C}$ , a destructive interference occurs in the same spectral region for both molecules, corresponding to  $n = 1$  for N<sub>2</sub>O and  $n = 0$  for C<sub>2</sub>H<sub>2</sub>.

Fig. 1(a) and 2(a) show two peculiar advantages related to the exploitation of mid-IR driving pulses for HHG. Indeed the harmonic cutoff extension related to the increase in the ponderomotive energy with respect to standard Ti:sapphire sources allows the observation of spectral features as the harmonic enhancement for high photon energy visible in N<sub>2</sub>O in correspondence of the revival peak. In the framework of the above mentioned two-center model, this feature can be attributed to the appearance of a constructive interference in that spectral region. Moreover, for the same emitted photon energy, mid-IR driving wavelengths require a lower pulse peak intensity thus reducing the ionization saturation in species with a relatively low ionization potential, such as C<sub>2</sub>H<sub>2</sub> ( $I_p = 11.4 \text{ eV}$ ).

## 4 Reconstruction of single molecule XUV emission

From the experimental data reported in Fig. 1(a) and 2(a) it is possible to retrieve structural information on the target molecule following the approach introduced by Vozzi *et al.*<sup>25</sup> Fig. 3(a) and 4(a) show the same experimental results presented in Fig. 1(a) and 2(a), in which the harmonic structure due to the periodic re-collision of the electron wave-packet has been filtered out. These results have been exploited for the reconstruction of the XUV field emitted from a single molecule and projected on the polarization direction of the aligning field as a function of the angle between the molecular axis and the driving polarization direction. The reconstruction is based on a combination of a phase-retrieval algorithm and a Kaczmarz algorithm.<sup>28</sup> The main idea behind this approach is that the macroscopic XUV emission is the coherent superposition of the XUV field emitted by all molecules weighted with their angular distribution. This distribution changes along the revival in a predictable way, hence the sequence of harmonic emission contains enough information for the reconstruction of the harmonic electric field in amplitude and phase.

The result of this reconstruction is shown in Fig. 5 for N<sub>2</sub>O and in Fig. 6 for C<sub>2</sub>H<sub>2</sub>. In both figures, panel (a) reports the amplitude of the XUV field and panel (b) shows the corresponding phase. In N<sub>2</sub>O there is a clear phase jump of about 2 rad, that changes its position with the photon energy and molecular alignment. This phase jump corresponds to a minimum in the XUV amplitude and its position is in good agreement with the prediction of the naive two-center model introduced above, which is shown as a dashed line in the figure. It is worth noting that the reconstruction technique is based on the interference of XUV emission from different molecular orientations, thus the phase can be retrieved as a function of  $\theta$  at a fixed XUV photon energy. In order to retrieve the phase relationship between contributions at neighboring energies it is necessary to



**Fig. 3** (a) Sequence of XUV spectra measured in  $\text{N}_2\text{O}$  as a function of the emitted photon energy and delay between the aligning and the driving pulse; the harmonic structure has been filtered out. Retrieved macroscopic harmonic emission amplitude (b) and phase (c) corresponding to the data reported in (a).

introduce an *a priori* condition that can be derived from theoretical considerations or experimental measurements. In the case of  $\text{N}_2\text{O}$  we imposed a flat spectral phase of the macroscopic harmonic emission for the delay corresponding to the molecular anti-alignment. This condition was chosen in analogy with the  $\text{CO}_2$  case<sup>25</sup> due to the similarity between the two HOMOs as discussed in the previous section. The results of this assumption can be observed in Fig. 3, where the reconstructed amplitude (b) and phase (c) of the macroscopic XUV emission from  $\text{N}_2\text{O}$  are reported. The retrieved amplitude is in good agreement with the experimental data (Fig. 3(a)). The phase of the macroscopic emission shows a steep change of about 2 rad around 50 eV at the delay  $\tau$  corresponding to the maximum alignment.

In the case of  $\text{C}_2\text{H}_2$  we followed the same approach in the retrieval procedure. We imposed in this case a flat spectral phase for the macroscopic harmonic emission at the delay  $\tau$  corresponding to the molecular alignment. This assumption was necessary in order to complete the retrieval procedure, but it is arbitrary and not supported by theoretical models; it could be however improved by changing the retrieving condition according to an experimental spectral phase measurement. This kind of experiment can be performed for example by RABBIT technique at a given alignment delay.<sup>9</sup> The retrieved single molecule XUV emission in  $\text{C}_2\text{H}_2$ , shown in Fig. 6, is very different from the one reported for  $\text{N}_2\text{O}$ . In particular a strong contribution comes from molecules with perpendicular orientation with respect to the driving field polarization direction. In the retrieved

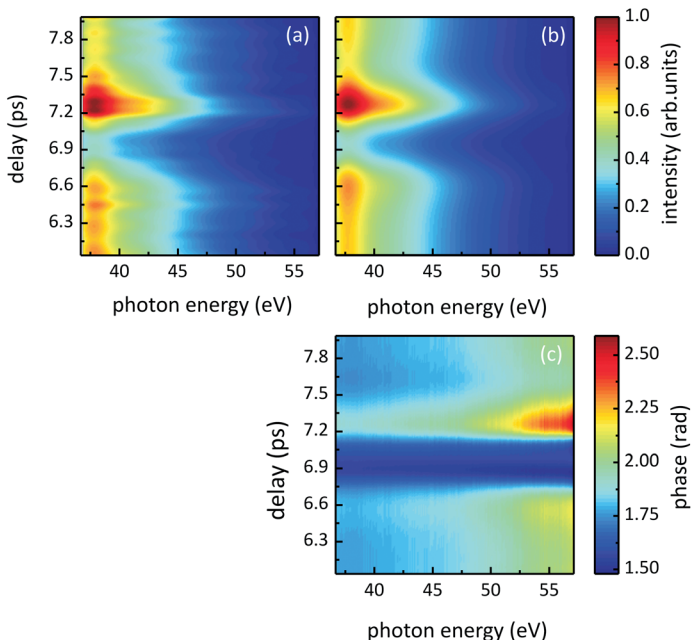


**Fig. 4** (a) Sequence of XUV spectra measured in  $\text{C}_2\text{H}_2$  as a function of the emitted photon energy and delay between the aligning and the driving pulse; the harmonic structure has been filtered out. Retrieved macroscopic harmonic emission amplitude (b) and phase (c) corresponding to the data reported in (a).

phase (Fig. 6(c)) two phase jumps are clearly observed. The first one appears for small alignment angles and roughly follows the prediction of the two-center model. The second jump appears at large alignment angles and may be attributed to the shape of the HOMO seen by the re-colliding electron. However, since the reconstruction is based on the arbitrary assumption of a flat macroscopic spectral phase at the alignment delay, the retrieved outcomes should be considered preliminary. In spite of this, the retrieved macroscopic XUV amplitude (Fig. 4(b)) is in fair agreement with the experimental results.

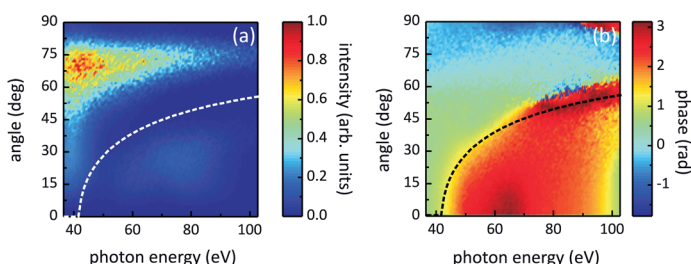


**Fig. 5** Retrieved single molecule XUV emission map in  $\text{N}_2\text{O}$  as a function of emitted photon energy and the angle between the molecular axis and the aligning beam polarization direction in amplitude (a) and phase (b). Dashed lines show the position of the destructive interference predicted by the two-center model.

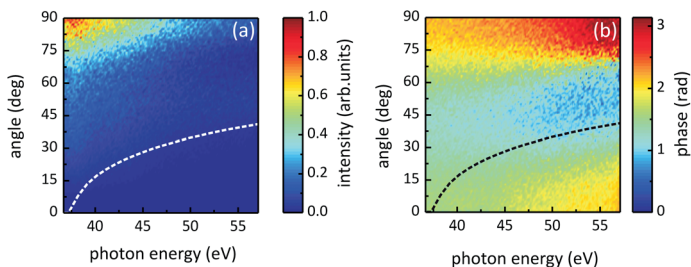


**Fig. 6** Retrieved single molecule XUV emission map in  $\text{C}_2\text{H}_2$  as a function of emitted photon energy and the angle between the molecular axis and the aligning beam polarization direction in amplitude (a) and phase (b). Dashed lines show the position of the destructive interference predicted by the two-center model.

## 5 Molecular orbital tomography

The results reported in the previous section can be used for the two-dimensional reconstruction of the molecular orbitals, following the tomographic procedure proposed by Itatani *et al.*<sup>5</sup> and extended by Vozzi *et al.*<sup>25</sup> However to proceed with this tomographic reconstruction, it is necessary to rule out the occurrence of multi-electron effects in HHG. A simple experimental procedure to check whether spectral modulations in harmonic emission are due to multi-electron effects is to change the driving field intensity. As shown by Smirnova *et al.*,<sup>3</sup> one expects all the features due to multi-electron effects to shift with the driving field intensity. Fig. 7 shows the harmonic spectra acquired in aligned  $\text{N}_2\text{O}$  for a delay  $\tau$  corresponding to the maximum of the alignment for different values of the driving intensity. The spectral minimum associated to the phase change retrieved in Fig. 5(b) appears always around 55 eV and does not shift with the driving intensity, as already observed by Rupenyan *et al.*<sup>29</sup> in similar experimental conditions. This behavior guarantees that the main spectral features in the harmonic emission are mainly dictated by the HOMO structure. This consistency check allowed us to exploit the retrieved single molecule harmonic emission for the reconstruction of the  $\text{N}_2\text{O}$

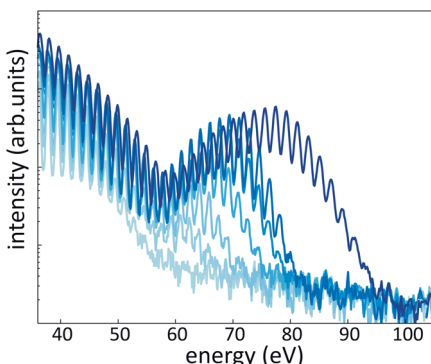


**Fig. 7** Harmonic spectra generated in  $\text{N}_2\text{O}$  at the delay  $\tau$  corresponding to the maximum molecular alignment for several driving peak intensities  $I$  between 1 and  $1.7 \times 10^{14} \text{ W cm}^{-2}$ .

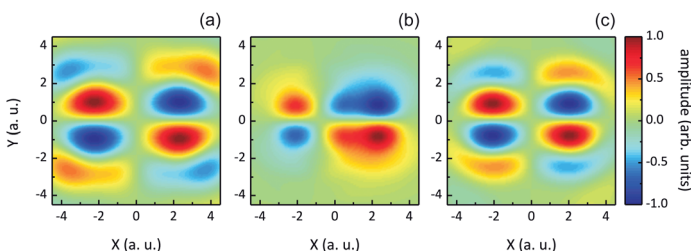


**Fig. 8** (a) Highest occupied molecular orbital of  $\text{N}_2\text{O}$  as retrieved from the single molecule XUV emission map. (b) Highest occupied molecular orbital of  $\text{N}_2\text{O}$  calculated with a quantum chemistry program.<sup>30</sup> (c)  $\text{N}_2\text{O}$  HOMO calculated averaging over the two possible orientations of the molecular axis and considering the filtering in spectral domain corresponding to the experimental conditions.

orbital. The result is shown in Fig. 8(a). Fig. 8(b) shows the  $\text{N}_2\text{O}$  orbital calculated with a quantum chemistry program.<sup>30</sup> Even if the overall dimension of the molecular orbital is well reproduced, the asymmetry of this orbital is very clear and cannot be addressed by the tomographic reconstruction, since in the experiment the molecules were aligned but not oriented. Another departure of the retrieved orbital with respect to the calculated one is the presence of side lobes, that can be attributed to the limited working range of the XUV spectrometer used in these experiments. Since there is a correspondence between the energy range of harmonic emission and the spatial frequency domain, the limited spectral range collectible in the experiment corresponds to a spatial filtering in the Fourier domain, which gives raise to such lobes. These observations are further confirmed by Fig. 8(c), which shows the calculated HOMO corresponding to the average between the two possible orientations of  $\text{N}_2\text{O}$  molecular axis and takes into account the limited spectral bandwidth available in the experiment. The features of this fictitious orbital are in very good agreement with the reconstruction of Fig. 8(a). It is worth noting that such limitations can be overcome by extending the acquired spectral range over all the XUV emission and by exploiting all-optical impulsive techniques for the orientation of polar molecules, such as the one demonstrated by Frumker *et al.*<sup>16,17</sup>

Differently from the case of  $\text{N}_2\text{O}$ , in  $\text{C}_2\text{H}_2$  it is not possible to easily rule out the multi-electron contributions. Because of the smaller cutoff energy, the

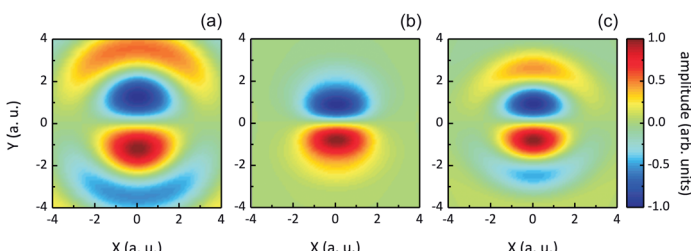


**Fig. 9** (a) Highest occupied molecular orbital of  $\text{C}_2\text{H}_2$  as retrieved from the single molecule XUV emission map. (b) Highest occupied molecular orbital of  $\text{C}_2\text{H}_2$  calculated with a quantum chemistry program.<sup>30</sup> (c)  $\text{C}_2\text{H}_2$  HOMO calculated considering filtering in the spectral domain corresponding to the experimental conditions.

experimental approach applied in the case of N<sub>2</sub>O for the exclusion of multi-electron contribution is not feasible. Nevertheless the application of the tomographic approach to the single molecule emission maps shown in Fig. 6 provides interesting results. We show in Fig. 9(a) the retrieved C<sub>2</sub>H<sub>2</sub> HOMO. Also in this case, a comparison with the result calculated with a quantum chemistry program (see Fig. 9(b)) shows a good agreement in the overall shape of the orbital. Again the additional lobes are related to the limited harmonic range detected in the experimental acquisition, as can be seen in Fig. 9(c) where the orbital is calculated taking into account spectral filtering.

## 6 Conclusions

Since the pioneering work of Itatani *et al.* on molecular orbital imaging, the impressive advances in laser technologies have given access to new mid-IR sources for driving HHG and pushing the harmonic emission far towards the soft-X-ray range. These sources allowed the application of HHG spectroscopy to fragile molecules, such as hydrocarbons, which can be considered prototypes for the study of ubiquitous phenomena in chemistry and materials science. In this work we showed the application of molecular orbital reconstruction based on HHG to non-trivial samples, such as N<sub>2</sub>O and C<sub>2</sub>H<sub>2</sub>. These results, though requiring further improvements, demonstrate the capability of molecular orbital tomography and represent the first step towards the imaging of dynamical processes in complex molecules.

## Acknowledgements

The research leading to these results has received funding from the LASERLAB-EUROPE (grant agreement no. 284464, EC Seventh Framework Programme), from the ERC Starting Research Grant UDYNI (grant agreement no. 307964, EC Seventh Framework Programme) and from the Italian Ministry of Research and Education (ELI project – ESFRI Roadmap).

## References

- 1 P. B. Corkum, *Phys. Rev. Lett.*, 1993, **71**, 1994–1997.
- 2 S. Baker, J. Robinson, C. Haworth, H. Teng, R. Smith, C. Chirila, M. Lein, J. Tisch and J. Marangos, *Science*, 2006, **312**, 424–427.
- 3 O. Smirnova, Y. Mairesse, S. Patchkovskii, N. Dudovich, D. Villeneuve, P. Corkum and M. Y. Ivanov, *Nature*, 2009, **460**, 972–977.
- 4 S. Haessler, J. Caillat, W. Boutu, C. Giovanetti-Teixeira, T. Ruchon, T. Auguste, Z. Diveki, P. Breger, A. Maquet, B. Carre, R. Taieb and P. Salieres, *Nat. Phys.*, 2010, **6**, 200–206.
- 5 J. Itatani, J. Levesque, D. Zeidler, H. Niikura, H. Pepin, J. Kieffer, P. Corkum and D. Villeneuve, *Nature*, 2004, **432**, 867–871.
- 6 T. Kanai, S. Minemoto and H. Sakai, *Nature*, 2005, **435**, 470–474.
- 7 C. Vozzi, F. Calegari, E. Benedetti, J. Caumes, G. Sansone, S. Stagira, M. Nisoli, R. Torres, E. Heesel, N. Kajumba, J. Marangos, C. Altucci and R. Velotta, *Phys. Rev. Lett.*, 2005, **95**, 153902.
- 8 A.-T. Le, R. R. Lucchese, M. T. Lee and C. D. Lin, *Phys. Rev. Lett.*, 2009, **102**, 203001.

- 9 W. Boutu, S. Haessler, H. Merdji, P. Breger, G. Waters, M. Stankiewicz, L. J. Frasinski, R. Taieb, J. Caillat, A. Maquet, P. Monchicourt, B. Carre and P. Salieres, *Nat. Phys.*, 2008, **4**, 545–549.
- 10 J. Levesque, Y. Mairesse, N. Dudovich, H. Pépin, J.-C. Kieffer, P. B. Corkum and D. M. Villeneuve, *Phys. Rev. Lett.*, 2007, **99**, 243001.
- 11 K. Miyazaki, M. Kaku, G. Miyaji, A. Abdurrouf and F. H. M. Faisal, *Phys. Rev. Lett.*, 2005, **95**, 243903.
- 12 W. Li, X. Zhou, R. Lock, S. Patchkovskii, A. Stolow, H. C. Kapteyn and M. M. Murnane, *Science*, 2008, **322**, 1207–1211.
- 13 Z. B. Walters, S. Tonzani and C. H. Greene, *J. Phys. Chem. A*, 2008, **112**, 9439–9447.
- 14 H. Stapelfeldt and T. Seideman, *Rev. Mod. Phys.*, 2003, **75**, 543–557.
- 15 S. De, I. Znakovskaya, D. Ray, F. Anis, N. G. Johnson, I. A. Bocharova, M. Magrakvelidze, B. D. Esry, C. L. Cocke, I. V. Litvinyuk and M. F. Kling, *Phys. Rev. Lett.*, 2009, **103**, 153002.
- 16 E. Frumker, C. T. Hebeisen, N. Kajumba, J. B. Bertrand, H. J. Woerner, M. Spanner, D. M. Villeneuve, A. Naumov and P. B. Corkum, *Phys. Rev. Lett.*, 2012, **109**, 113901.
- 17 E. Frumker, N. Kajumba, J. B. Bertrand, H. J. Wörner, C. T. Hebeisen, P. Hockett, M. Spanner, S. Patchkovskii, G. G. Paulus, D. M. Villeneuve, A. Naumov and P. B. Corkum, *Phys. Rev. Lett.*, 2012, **109**, 233904.
- 18 M. Spanner, S. Patchkovskii, E. Frumker and P. Corkum, *Phys. Rev. Lett.*, 2012, **109**, 113001.
- 19 E. J. Takahashi, T. Kanai, K. L. Ishikawa, Y. Nabekawa and K. Midorikawa, *Phys. Rev. Lett.*, 2008, **101**, 253901.
- 20 C. Vozzi, R. Torres, M. Negro, L. Brugnera, T. Siegel, C. Altucci, R. Velotta, F. Frassetto, L. Poletto, P. Villoresi, S. De Silvestri, S. Stagira and J. P. Marangos, *Appl. Phys. Lett.*, 2010, **97**, 241103.
- 21 C. Vozzi, F. Calegari, M. Negro, F. Frassetto, L. Poletto, G. Sansone, P. Villoresi, M. Nisoli, S. De Silvestri and S. Stagira, *J. Mod. Opt.*, 2010, **57**, 1008–1013.
- 22 C. Vozzi, F. Calegari, F. Frassetto, M. Negro, L. Poletto, G. Sansone, P. Villoresi, M. Nisoli, S. Silvestri and S. Stagira, *Laser Phys.*, 2010, **20**, 1019–1027.
- 23 T. Popmintchev, M.-C. Chen, D. Popmintchev, P. Arpin, S. Brown, S. Ališauskas, G. Andriukaitis, T. Balčiunas, O. D. Mücke, A. Pugzlys, A. Baltuška, B. Shim, S. E. Schrauth, A. Gaeta, C. Hernández-García, L. Plaja, A. Becker, A. Jaron-Becker, M. M. Murnane and H. C. Kapteyn, *Science*, 2012, **336**, 1287–1291.
- 24 C. Vozzi, F. Calegari, E. Benedetti, S. Gasilov, G. Sansone, G. Cerullo, M. Nisoli, S. De Silvestri and S. Stagira, *Opt. Lett.*, 2007, **32**, 2957–2959.
- 25 C. Vozzi, M. Negro, F. Calegari, G. Sansone, M. Nisoli, S. De Silvestri and S. Stagira, *Nat. Phys.*, 2011, **7**, 822–826.
- 26 L. Poletto, G. Tondello and P. Villoresi, *Rev. Sci. Instrum.*, 2001, **72**, 2868–2874.
- 27 M. Lein, N. Hay, R. Velotta, J. Marangos and P. Knight, *Phys. Rev. A: At., Mol., Opt. Phys.*, 2002, **66**, 023805.
- 28 C. Popa and R. Zdunek, *Math. Comput. Simul.*, 2004, **65**, 579–598.
- 29 A. Rupenyan, P. M. Kraus, J. Schneider and H. J. Wörner, *Phys. Rev. A: At., Mol., Opt. Phys.*, 2013, **87**, 031401(R).
- 30 DALTON, a molecular electronic structure program Release 2.0 (2005) see <http://www.kjemi.uio.no/software/dalton/dalton.html>.